Chem

CellPress

Article

# Self-Assembled Molecular-Electronic Films Controlled by Room Temperature Quantum Interference

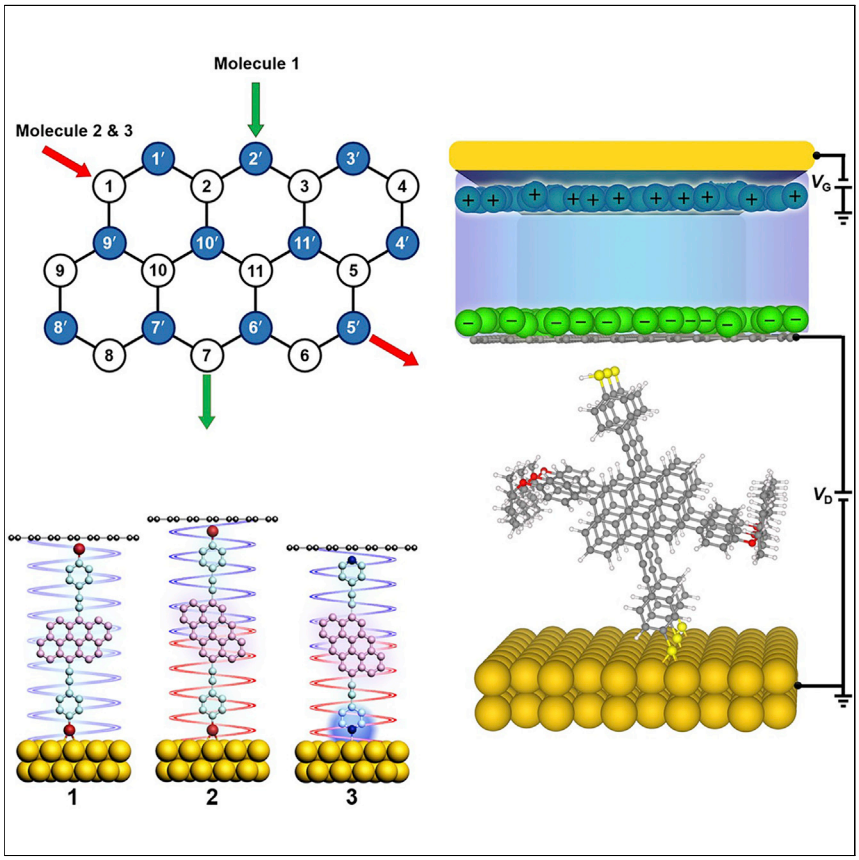


Molecular-scale electronics is a branch of nanotechnology, which utilizes molecules as electronic components. Here, we demonstrate that room-temperature quantum interference (QI) effects identified in single molecules can be translated into ultra-thin-film materials. This breakthrough opens up avenues for exploiting QI in the design of new materials with enhanced electrical, thermal, and sensing functionality. Field effect control using an ionic liquid gate demonstrates that QI can be used to optimize the on-off ratio of ultra-thin-film transistors.

Marjan Famili, Chuancheng Jia, Xunshan Liu, ..., Shi-Xia Liu, Colin J. Lambert, Xiangfeng Duan

yhuang@seas.ucla.edu (Y.H.)
liu@dcb.unibe.ch (S.-X.L.)
c.lambert@lancaster.ac.uk (C.J.L.)
xduan@chem.ucla.edu (X.D.)

## HIGHLIGHTS

A vertical tunneling organic transistor on graphene

Room-temperature intra-molecular quantum interference in self-assembled monolayers

Field effect tuning of the energy levels of a self-assembled monolayer on graphene

Quantum interference optimizes the on-off ratio of ultra-thin-film transistors

Famili et al., Chem 5, 474–484
February 14, 2019 
https://doi.org/10.1016/j.chempr.2018.12.008

Chem

CellPress

Article

# Self-Assembled Molecular-Electronic Films Controlled by Room Temperature Quantum Interference

Marjan Famili,[2,7] Chuancheng Jia,[1,7] Xunshan Liu,[3,7] Peiqi Wang,[1,4] Iain M. Grace,[2] Jian Guo,[4] Yuan Liu,[4,5] Ziying Feng,[1] Yiliu Wang,[1] Zipeng Zhao,[4] Silvio Decurtins,[3] Robert Häner,[3] Yu Huang,[4,6,*] Shi-Xia Liu,[3,*] Colin J. Lambert,[2,8,*] and Xiangfeng Duan[1,6,*]

## SUMMARY

**If single-molecule, room-temperature, quantum interference (QI) effects could be translated into massively parallel arrays of molecules located between planar electrodes, QI-controlled molecular transistors would become available as building blocks for future electronic devices. Here, we demonstrate unequivocal signatures of room-temperature QI in vertical tunneling transistors, formed from self-assembled monolayers (SAMs), with stable room-temperature switching operations. As a result of constructive QI effects, the conductances of the junctions formed from anthanthrene-based molecules with two different connectivities differ by a factor of 34, which can further increase to 173 by controlling the molecule-electrode interface with different terminal groups. Field-effect control is achieved using an ionic liquid gate, whose strong vertical electric field penetrates through the graphene layer and tunes the energy levels of the SAMs. The resulting room-temperature on-off current ratio of the lowest-conductance SAMs can reach up to 306, about one order of magnitude higher than that of the highest-conductance SAMs.**

## INTRODUCTION

Molecular electronics represent an attractive alternative for future electronic devices with potential to deliver logic gates, sensors, memories, and thermoelectric energy harvesters with ultra-low power requirements and sub-10 nm device footprints.[1–4] Single-molecule electronic junctions have been investigated intensively over the past decade, not only as stepping stones toward functional devices and circuits made from collections of molecules but also because their room-temperature electrical conductance is controlled by quantum interference (QI).[5–15] Figure 1A illustrates an example of a non-classical QI effect, in a graphene-like (anthanthrene) molecular core, when an electrical current is injected and collected via the green arrows, or alternatively, via the red arrows. If the core behaved like a classical resistor network, then the electrical conductance for these two connectivities would be approximately equal. In contrast, theory predicts and experiments confirm[16–18] that the room temperature, single-molecule, low-bias electrical conductance ($G_1$) for the green (7,2′) connectivity is approximately two orders of magnitude larger than the conductance ($G_2$) of the red (1,5′) connectivity. This is a clear signature of their different degrees of constructive QI (Figure S5). The chemical realization of the green connectivity is molecule **1** (Figure 1B), in which the terminal groups attached to the electrodes inject a current into the anthanthrene core via triple bonds (Scheme S1). Similarly, molecules **2** and **3** are realizations of the red

## The Bigger Picture

Molecular electronics represent an attractive alternative for future electronic devices with rich functionalities beyond current scaling limits of silicon-based electronics. Compared with solid-state quantum technologies, where quantum effects are confined to low temperatures, molecular electronics are advantageous because quantum effects can be realized at room temperature. Here, we report the realization of room-temperature quantum interference (QI) effects on the electrical conductance of molecules in self-assembled monolayers, demonstrating that it is feasible to utilize QI in the design of new functional, ultra-thin film materials and devices. The combination of the modification of molecular terminal groups with the above QI effect leads to a QI-driven vertical molecular transistor with a high on-off ratio. The broader significance is that this work opens up appealing opportunities for both new scientific exploration and technological innovation in molecular electronics.

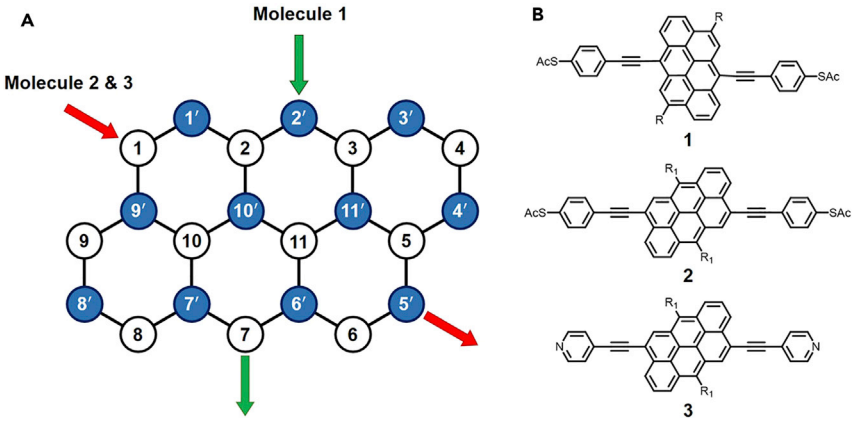


**Figure 1. Structures of Studied Molecules**

(A) Sketch of an anthanthrene core with connectivities 7,2′ and 1,5′ (the numbering system is chosen for mathematical convenience and does not coincide with standard chemical notation).

(B) Chemical realizations of molecules with anthanthrene cores. Molecule **1** corresponds to the 7,2′ connectivity, whereas molecules **2** and **3** correspond to the 1,5′ connectivity. R = 4-(2-ethylhexyloxy) phenyl, $R_1$ = -$OC_8H_{17}$.

connectivity, with different terminal groups, which can further control the interfacial coupling and energy-level alignment between the molecule and electrode.[19,20] Our aim is to create a self-assembled monolayer (SAM)-based molecular tunneling transistor from these molecules and to demonstrate that these single-molecule signatures of QI can be realized in SAM-based devices. Indeed, we found that the electrical conductance of the SAM formed from molecule **1** is significantly higher than that of the SAM formed from either molecule **2** or **3**. Furthermore, by applying an external gate, we are able to assess their different field-effect performances.

## RESULTS

### Construction of the Devices

In contrast to molecular tunneling transistors fabricated by placing a solid back gate[21] or electrochemical gate[22,23] to the side of molecular junctions, which can typically only operate stably only at cryogenic temperatures, here we utilize a vertical molecular tunneling transistor with stable room-temperature operation, based on a gate-modulated graphene/SAM/gold cross-plane vertical heterostructure.[24,25] The binding geometry of the molecules in the SAM are fixed[26] by the terminal anchor groups to the gold electrode and the inter-molecular interactions in the SAM, which promote a stable charge transport through the molecular junctions. A strong gating electric field, generated from the electrical double layer (EDL) of ionic liquid,[27] is vertically applied to the graphene/SAM/gold junctions (Figure 2A). As a result of the partial electrostatic transparency of graphene,[28] the applied electric field penetrates through the graphene layer and tunes the energy levels of the SAM relative to the Fermi energy of gold ($E_F^{gold}$), resulting in effective gate control and a significant conductance modulation in the molecular transistors.

The fabrication processes of the vertical molecular tunnel transistors are shown schematically in the Supplemental Information (Figure S1). Figures 2B and 2C show a schematic illustration of the structure and an optical photograph of the fabricated device. An ultra-flat gold film is deposited on the exposed, conducting silicon surface into a small hole at the center of a silicon/$SiO_2$ chip, which is then connected to a metal electrode at the corner and used as the source electrode. A SAM of

[1]Department of Chemistry and Biochemistry, University of California, Los Angeles, Los Angeles, CA 90095, USA

[2]Physics Department, Lancaster University, Lancaster LA1 4YB, UK

[3]Department of Chemistry and Biochemistry, University of Bern, Bern CH-3012, Switzerland

[4]Department of Materials Science and Engineering, University of California, Los Angeles, Los Angeles, CA 90095, USA

[5]School of Physics and Electronics, Key Laboratory for Micro-Nano Optoelectronic Devices of Ministry of Education, Hunan University, Changsha 410082, China

[6]California NanoSystems Institute, University of California, Los Angeles, Los Angeles, CA 90095, USA

[7]These authors contributed equally

[8]Lead Contact

*Correspondence: yhuang@seas.ucla.edu (Y.H.), liu@dcb.unibe.ch (S.-X.L.), c.lambert@lancaster.ac.uk (C.J.L.), xduan@chem.ucla.edu (X.D.)

https://doi.org/10.1016/j.chempr.2018.12.008

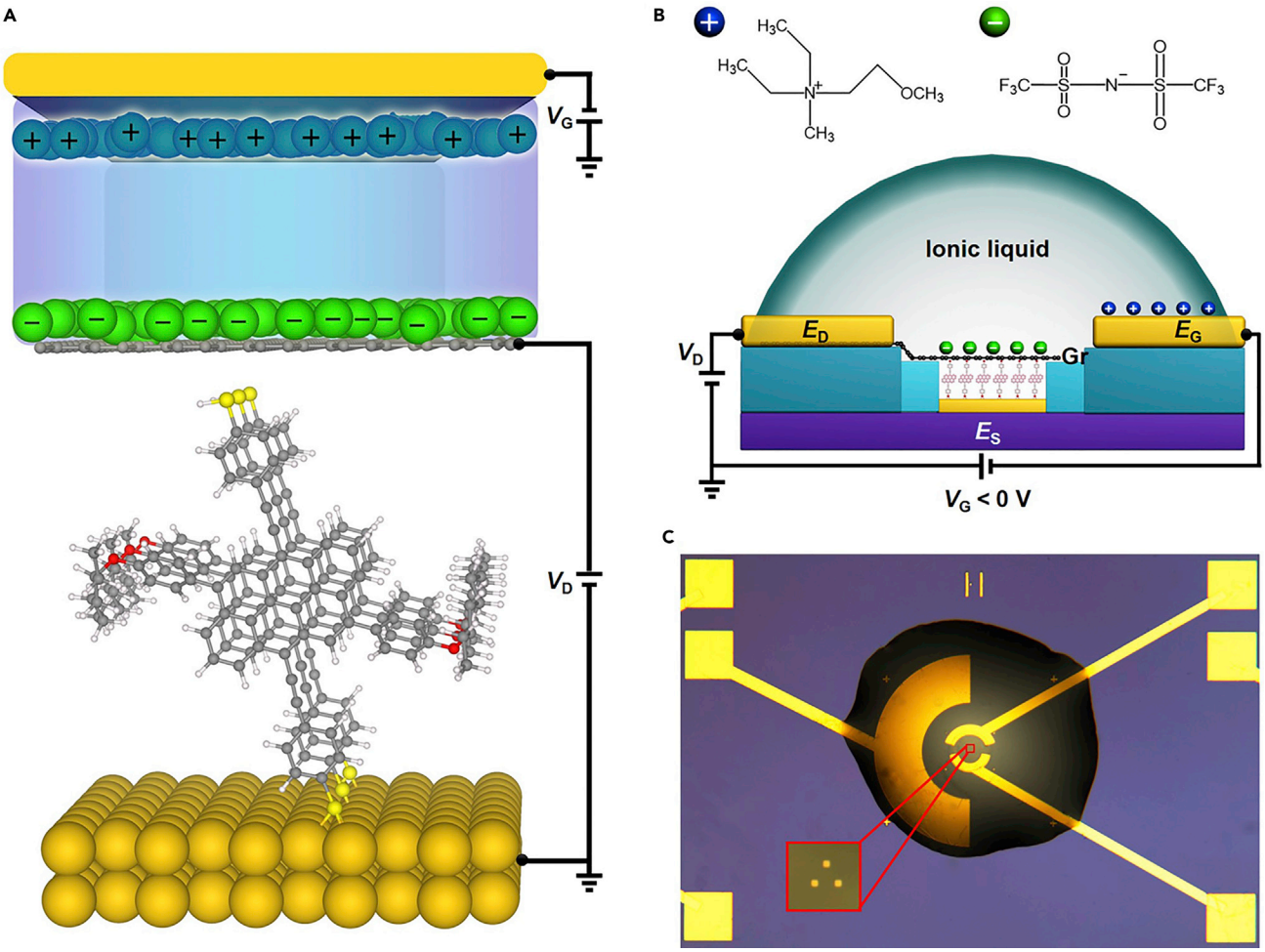


**Figure 2. Schematic Illustration of the Vertical Molecular Tunneling Transistor**

(A and B) Schematic illustration for the setup of the device with a vertical ionic liquid gate through graphene layer to SAMs and molecular structures for $DEME^+$ cation and $TFSI^-$ anion.

(C) Optical photograph of the device with the ionic liquid gate.

molecule **1**, **2**, or **3** (Figure 1B) is then functionalized on the Au film and confirmed by atomic force microscopy (AFM), X-ray photoelectron spectroscopy (XPS), and Raman characterization (Figures S2–S4). Chemical vapor deposition (CVD) grown single-layer graphene (SLG)[29] (Figure S4A) is then transferred and patterned on the top of the SAM. A drain electrode connecting with the graphene sheet and gate electrode is laid around the functional center. Finally, a small amount of diethylmethyl(2-methoxyethyl)ammonium bis(trifluoromethylsulfonyl)imide (DEME-TFSI) ionic liquid is dropped on the graphene/SAM/gold channel and gate electrode. Because the binding geometry and conformation of the molecules are fixed in SAMs,[26] and graphene electrodes prevent direct contact between the SAM and ionic liquid, stable devices can be realized with low noise operation at room temperature.

## Charge Transport in Molecular Junctions

In the absence of electrically active side chains, the ratio $\frac{G_1}{G_2}$ of the low-bias, single-molecule conductances of molecules **1** and **2** are predicted by a "magic number" table provided in Geng et al.[16], which yields $\frac{G_1}{G_2} = 81$ (Figure S5). This simple "magic ratio theory" illustrates how connectivity alone contributes to conductance ratios,

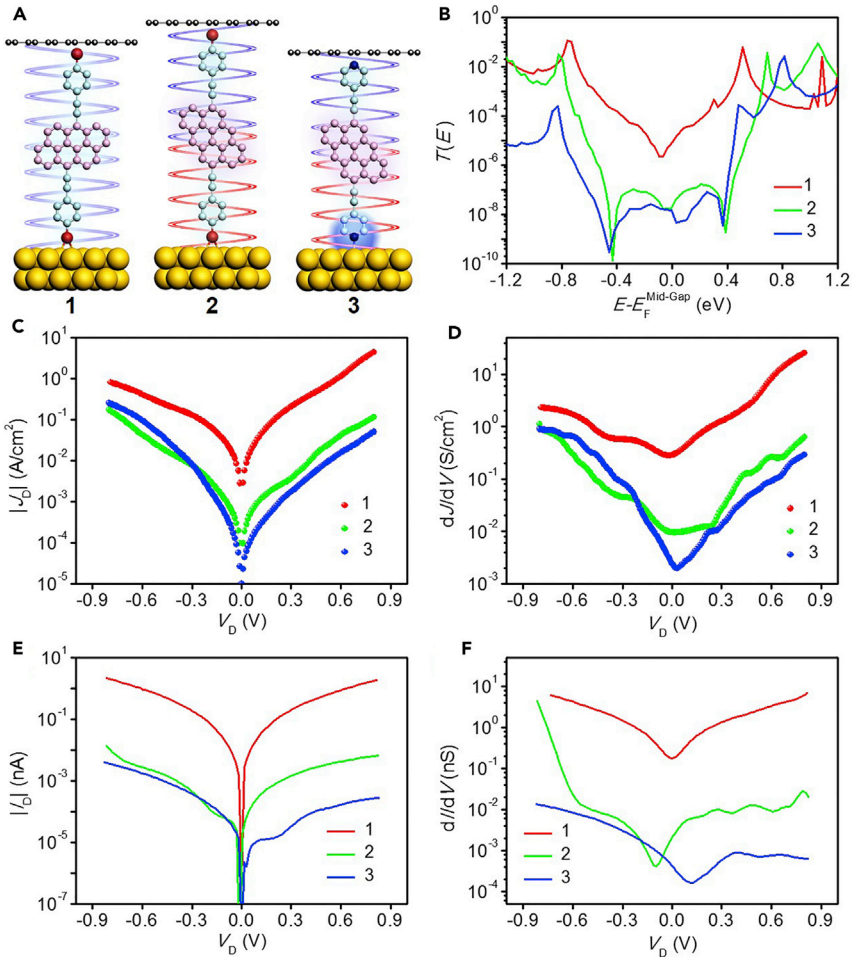


**Figure 3. Charge Transport in Molecular Junctions**

(A) Schematic illustration of the molecular junctions of molecules **1**, **2**, and **3**, where the side chains are hidden.

(B) Transmission functions $T(E)$ for molecules **1** (red), **2** (green), and **3** (blue).

(C) Plots of experimental current density ($J_D$) versus bias voltage ($V_D$) for molecules **1**, **2**, and **3**.

(D and E) Experimental differential conductance (dJ/dV) versus $V_D$. (E) Theoretical current ($I_D$) versus $V_D$.

(F) Theoretical differential conductance (d$I$/d$V$) versus $V_D$.

without including chemical effects or coulomb interactions. When the latter are included, recent studies indicate that the qualitative trend in the ratio is preserved (i.e., that $\frac{G_1}{G_2} \gg 1$), but the precise value should be calculated using *ab initio* methods.

Figure 3B shows the computed transmission coefficient for electrons passing through all three junctions. Previous comparison between findings from experiments and theory revealed that electron transport through single anthanthrene-based molecules attached to gold electrodes takes place near the middle of the energy gap between the highest occupied molecular orbital (HOMO) and the lowest unoccupied molecular orbital (LUMO).[16] Therefore, in the calculations presented below, the Fermi energy of the gold is located near the middle of the HOMO-LUMO gap, and all energy axes are plotted with respect to the mid-gap energy $E_F^{mid-Gap} = E_F^{Gold}$. The computed ratio of their transmission coefficients in graphene/molecule/gold junctions (Figure S7A) for molecules **2** and **1** at

$E = E_F^{Gold}$ is 116. It should be emphasized that both molecules exhibit constructive QI near their gap centers, and the conductance ratio arises from the different degrees of constructive QI associated with the different connectivities. Figure S6 illustrates that the constructive nature of the QI is also reflected in the molecular orbitals of molecules **2** and **1**. When the terminal groups of molecules are changed from thiol to pyridine, the transmission coefficient in the junctions of molecule **3** at $E = E_F^{Gold}$ is reduced to 1/7 of that for molecule **2**. This indicates that the QI effect acts in conjunction with the higher pyridine-gold interface resistance[30] to determine charge transport in the junctions.

The experimental current density ($J_D$) versus bias voltage ($V_D$) and the differential conductance (dJ/dV) versus $V_D$ are shown in Figures 3C and 3D. As predicted by the magic ratio theory, the current density ($J_D$) for the 1,5′ junction formed at molecule **2** is considerably lower than that of the 7,2′ junction formed at molecule **1**, especially near zero bias, which is consistent with the transmission coefficient characteristics of the respective molecules discussed above and the theoretical results (Figure 3E). With pyridine terminal groups at the 1,5′ junction, the $J_D$ for molecule **3** is further reduced, in agreement with the transmission functions.

The minimum values seen in the dJ/dV curves are associated with the Dirac point of the graphene, and their position relative to the zero $V_D$ indicates whether the graphene is p-doped or n-doped. In Figure 3D, the Dirac point for molecule **1** and **2** samples occurs at –0.03 V and –0.05 V respectively, indicating that graphene is slightly n-doped in the presence of the thiol-terminated SAMs. However, for molecule **3**, this minimum appears at 0.01V, suggesting p-doped graphene in the case of a pyridine anchor group. For this reason, in what follows, when comparing our calculated $T(E)$ with the findings from experiments, the band structure of the graphene is adjusted to place the Dirac point of each system at the experimental value.

For the experimental dJ/dV results (Figure 3D), the value of dJ/dV at zero bias for molecule **1** is 29 times larger than that of molecule **2**. From the statistics of 19 different experimental devices (Section S6 in Supplemental Information), the zero-bias differential conductance for molecule **1** is 34 times larger than that for molecule **2** (Table S1). This ratio is comparable with the value of 84 obtained from the theoretical results as shown in Figure 3F). It is also worth mentioning that for molecules **2** and **1**, junctions with gold/molecule/gold contacts (Figure S8), the conductance ratio at zero bias is $\frac{G_1}{G_2} = 203$, which indicates that the interfacial contacts play a role in determining the conductance ratio. After changing the terminal groups from thiol to pyridine to control the interfacial contacts, the zero-bias differential conductance for molecule **3** is 1/5.0 of that for molecule **2**, which is 1/5.1 from the statistics of 19 different experimental devices (Table S1). This value is also comparable with the calculated value of 1/8.7 (Figure 3F).

### Field Effect Properties of the Transistors

To probe the field effect performance of these molecular junctions, a DEME-TFSI ionic liquid was used for gating, which has a large electrochemical window, a high ionic conductivity, and a low freezing temperature for ion migration.[31] When a gate voltage ($V_G$) is applied to the gate electrode, a Helmholtz EDL self-organizing on the outside surface of the graphene layer (Figures 2A and 2B) generates a strong electric field up to ~ 10 MV/cm at the molecular junction.[27] The gate performances of three transistors were measured at room temperature (298 K). Figures 4A, 4D, and 4G show typical gate-dependent $J_D$-$V_D$ characteristics for molecules **1**, **2**, and **3**, respectively. Changing $V_G$ from –1 to 1 V greatly increases $J_D$ for negative $V_D$, while

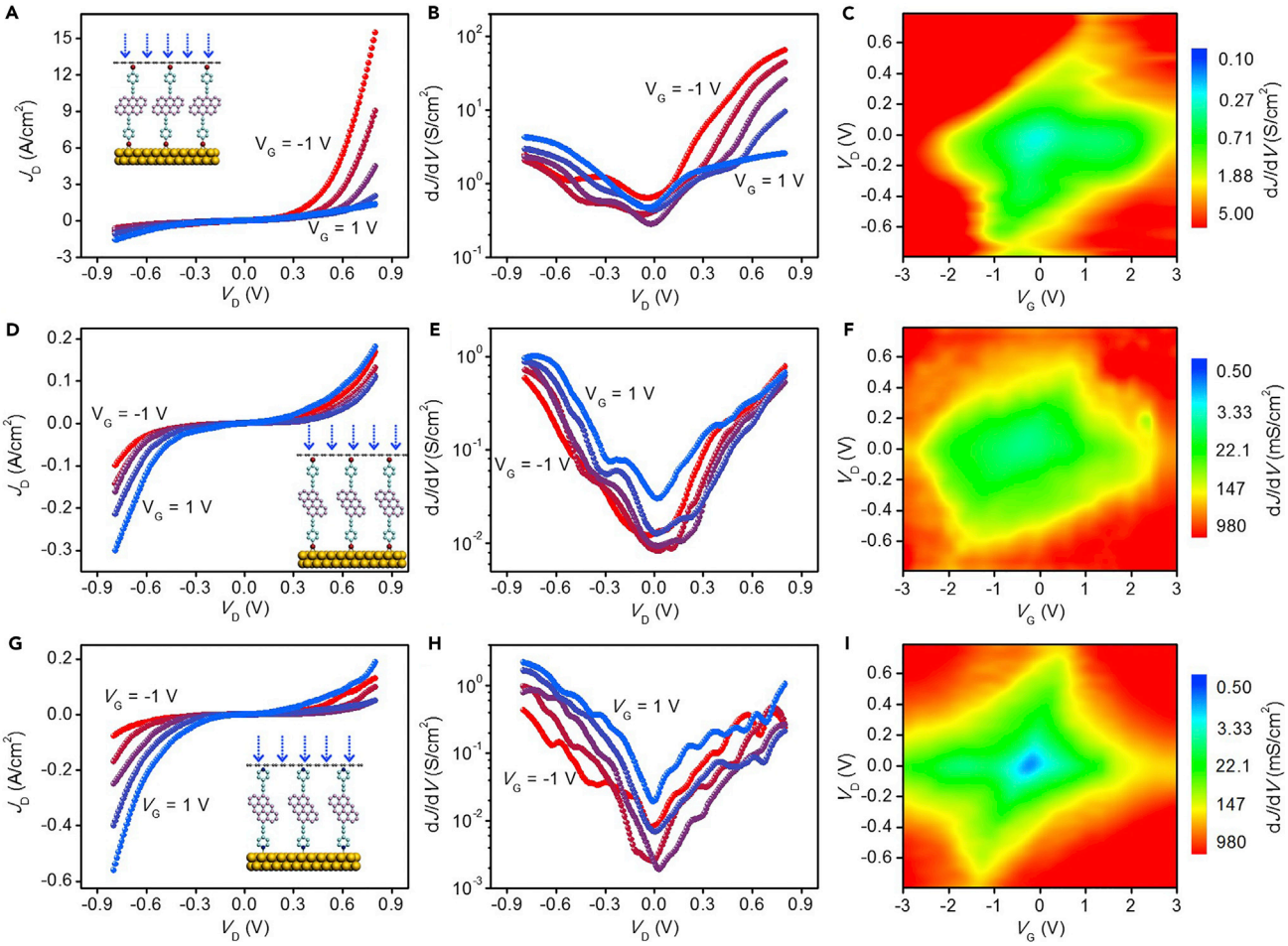


**Figure 4. Gating Charge Transport in Molecular Transistors**

(A, D, and G) $J_D$ versus $V_D$ characteristics for molecules **1** (A), **2** (D), and **3** (G) with gate voltage ($V_G$) changing from −1 to 1 V with steps of 0.5 V. Insets show schematics of the **1**, **2**, and **3** transistors with applied vertical electric field.

(B, E, and H) dJ/dV versus $V_D$ characteristics for molecules **1** (B), **2** (E), and **3** (H) with $V_G$ values changing from −1 to 1 V with steps of 0.5 V.

(C, F, and I) Two-dimensional visualization of dJ/dV versus $V_G$ and $V_D$ for molecules **1** (C), **2** (F), and **3** (I).

$J_D$ greatly decreases with $V_G$ for positive $V_D$, clearly demonstrating effective field-effect modulation of the molecular junctions (Section S7 in Supplemental Information).

Typical gate-dependent d$J$/d$V$-$V_D$ characteristics for molecules **1**, **2**, and **3** are shown in Figures 4B, 4E, and 4H. When the gate voltage is increased from −1 to 1 V, d$J$/d$V$-$V_D$ curves for all three junctions move in a positive direction along the $V_D$ axis, which reflects the gate-voltage dependent movement of the molecular orbital energy levels. Figures 4C, 4F, and 4I show two-dimensional visualizations of dJ/dV plotted versus $V_G$ and $V_D$ for molecules **1**, **2** and **3**, respectively. The oblique diamond-shaped low conductance region (green and blue) can be observed for all three transistors, which indicates off-resonant transport through the HOMO-LUMO gap. The red-orange high-conductance region outside the diamond is due to the conductive frontier molecular orbitals entering the bias window. The relative conductance change between the low conductance at the center region and the high conductance at the outside region for molecule **1** is considerably smaller than that for molecule **2**, which indicates the better gating tunability for molecule **1**. This agrees with the calculated $T(E)$ for molecules **1** and **2** (Figure 3B), as the

difference between off-resonant and resonant transport is more pronounced for molecule 2 in comparison to molecule 1. When comparing molecules 3 and 2, a lowest conductance region (blue) appears at the center of the diamond for molecule 3 (Figure 4F), corresponding to the calculated lowest off-resonant transmission of molecule 3 (Figure 3B), which further improves the gating tunability of molecule 3.

The conductance minima for molecule 1 are sharp features for all values of the applied gate voltage. However, in the case of molecule 2 (Figure 4E), the minimum at $V_G$ = 0 V is a broader feature, which splits into two sharper minima when the gate voltage is increased to 0.5 V and 1.0 V (for examples of other devices, see Figures S10–S27). This is in agreement with the calculated $T(E)$ for molecules 1 and 2 (Figure 3B). While $T_1$ has no features between the HOMO and LUMO apart from the Dirac point, $T_2$ has two sharp anti-resonances. For $V_G$ = 0, none of the anti-resonances are close enough to the Fermi energy to appear in the d$I$/d$V$ curves. By increasing the gate voltage, and hence the relative position of the anti-resonances to the Fermi energy, one of the anti-resonances is close enough to the Fermi-energy to be captured in the d$I$/d$V$. The lever arms in the theoretical model (see Theoretical Methods), which provide the best agreement between theory and experiment, are ($\alpha$ = 0.4, $\gamma$ = 0.25, and $\beta$ = 0.25).

## Working Mechanism of the Transistors

Figures 5A, 5D, and 5G show the $V_D$ dependence of $T(E)$ versus $E - E_F^{Gold}$ for molecules 1, 2, and 3. It is assumed that the energies of the molecular levels relative to $E_F^{Gold}$ are independent of $V_D$ and that positive (negative) bias voltage decreases (increases) the Dirac point relative to $E_F^{Gold}$ (Equation 1 in Supplemental Computational Methods). The current is computed using Equation 4 (see Supplemental Computational Methods) by evaluating individual transmission coefficients $T(E, V_D, V_G)$ at every $V_D$ value and computing the associated current. The d$I$/d$V$ curves are then obtained by differentiating the current with respect to $V_D$.

The $V_D$ and $V_G$ dependent transmission coefficient $T(E, V_D, V_G)$ was calculated using the quantum transport code Gollum[32] and the current obtained from Equation 4 (see Supplemental Computational Methods). The theoretical gate-dependent $I_D$-$V_D$ characteristics for molecule 2 (Figure 5E) reveal that when $V_G$ changes from −0.6 to 0.6 V, $I_D$ greatly increases with $V_G$ for negative $V_D$, whereas $I_D$ decreases with $V_G$ for positive $V_D$. A similar theoretical gate-dependent $I_D$-$V_D$ characteristic is also obtained for molecule 1 (Figure 5B), although the gate-dependent change in $I_D$ is smaller than that for molecule 2. Furthermore, from the gate-dependent d$I$/d$V$-$V_D$ characteristics for molecule 2 (Figure 5F), it can be observed that the d$I$/d$V$-$V_D$ curve shifts in a positive direction with $V_G$ changing from −0.6 to 0.6 V, especially for the lowest conductance points. For molecule 1, a similar gate-dependent d$I$/d$V$-$V_D$ curve is obtained, but with a relatively smaller amplitude (Figure 5C), in qualitative agreement with the experimental results (Figure 4). For molecule 3, gate-dependent $I_D$-$V_D$ (Figure 5H) and d$I$/d$V$-$V_D$ (Figure 5I) curves with a relatively larger amplitude can be observed, which are similar to molecule 2. Moreover, the lowest conductance minima appear in gate-dependent d$I$/d$V$-$V_D$ curves (Figure 5I), which is consistent with the experimental lowest conductance region (Figure 4I).

## Transfer Characteristics of the Transistors

Transfer characteristics, which are obtained by monitoring the current modulation with varying $V_G$ at a fixed $V_D$, are widely used for assessing transistor performance.[33] The $V_D$-dependent transfer characteristics for molecules 1, 2, and 3 were investigated both experimentally and theoretically. Experimental transfer characteristics

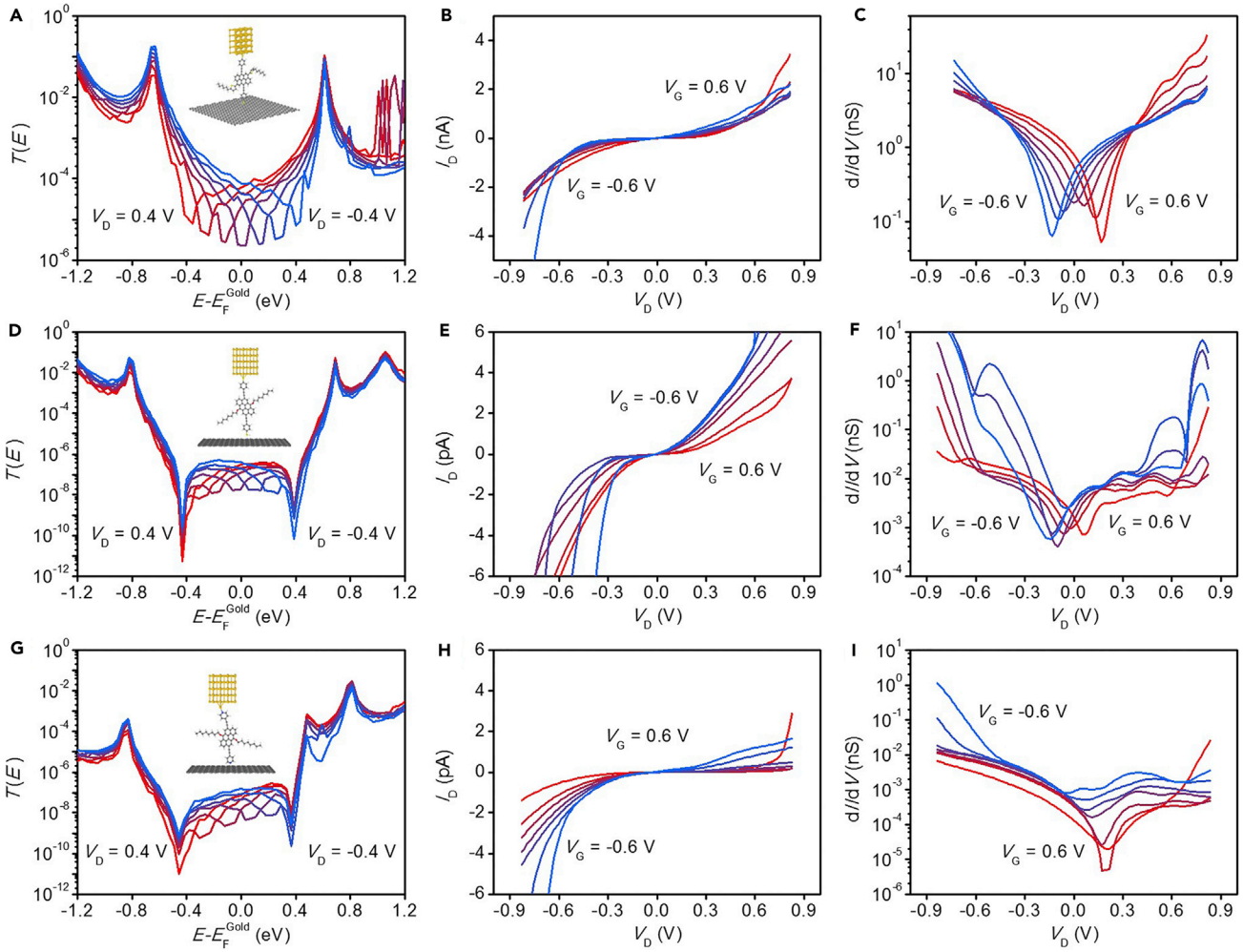


**Figure 5. Working Mechanism for Vertical Molecular Transistors**

(A, D, and G) Transmission coefficient $T(E)$ versus $E - E_F^{Gold}$ for molecular junction of 1 (A), 2 (D), and 3 (G) for $-0.4 < V_D < 0.4$ with steps of 0.13 V (red for $V_D = 0.4$ V). Insets show the structures of molecular junctions for simulation.

(B, E, and H) Gate-dependent theoretical $I_D$-$V_D$ characteristics of 1 (B), 2 (E), and 3 (H) for $-0.6 < V_G < 0.6$ with steps of 0.2 V (red for $V_G = 0.6$ V).

(C, F, and I) Gate-dependent theoretical $dI/dV$-$V_D$ characteristics for 1 (C), 2 (F), and 3 (I) for $-0.6 < V_G < 0.6$ with steps of 0.2 V (red for $V_G = 0.6$ V).

($J_D$-$V_G$) for molecule **1** at $V_D$ = –0.1, –0.2, –0.4, –0.6, and –0.8 V are shown in Figure 6A (for further devices see Figures S28–S33). It can be observed that the lowest current point at $V_D$ = –0.1 V is near $V_G$ = 0 V; and with the $V_D$ changing from –0.1 to –0.8 V, the lowest current point shifts to a more negative $V_D$. As the Dirac point of the graphene electrode dominates the conductance minima for molecule **1** (Figure 5A), such shifting of the lowest current point is due to the variation of the Dirac point of the graphene electrode. Specifically, with a more negative $V_D$, an increased negative $V_G$ is needed to move the central transmission dip of the junction to the middle of the bias window. This experimental phenomenon is also confirmed by the theoretical transfer characteristics ($I_D$-$V_G$) for molecule **1** (Figure 6D), as $V_D$ changes from –0.1 to –0.8 V. A similar behavior occurs for $J_D$-$V_G$ curves with positive $V_D$ (Figure S28A). The on-off ratio, which corresponds to the ratio between the highest and lowest currents in a $J_D$-$V_G$ curve, is up to 26 near $V_D$ = 0 V for molecule **1** (Figure S28B). In contrast, the highest on-off ratio for molecule **2** (Figure 6B) is increased to 105 near $V_D$ = 0 V (Figure S28D), which is about four times the value obtained for

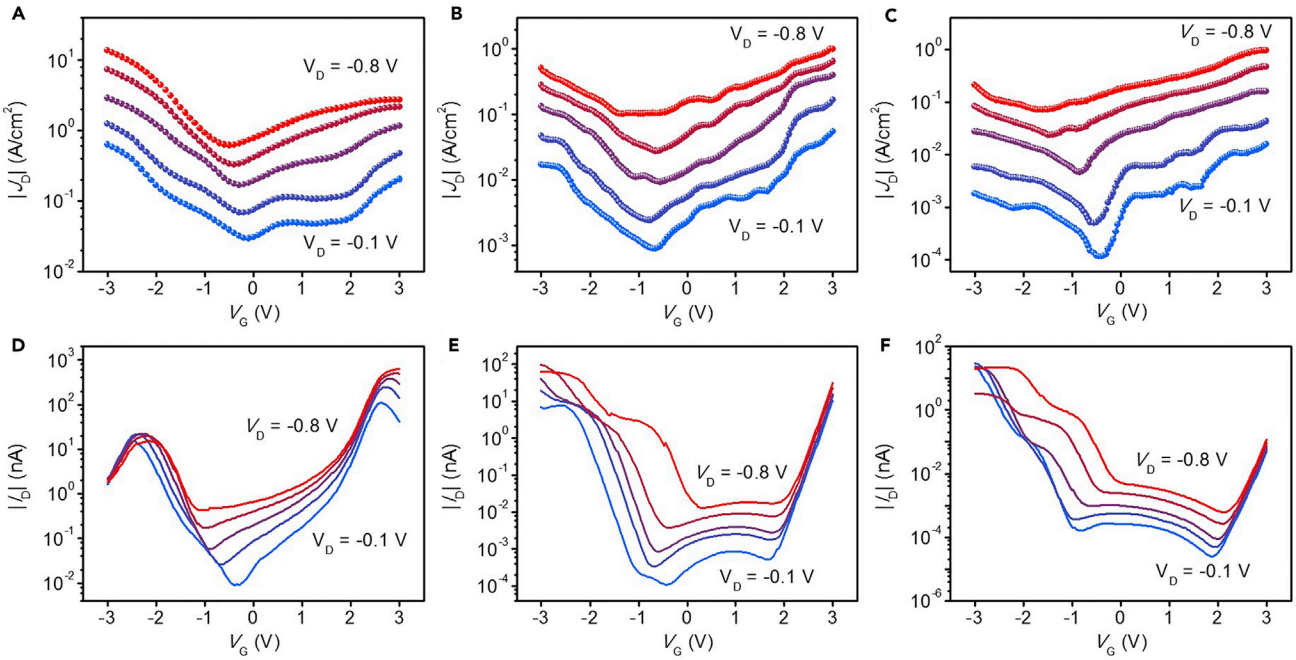


**Figure 6. Transfer Characteristics for the Vertical Molecular Transistors**

(A–C) Experimental transfer characteristics for molecules **1** (A), **2** (B), and **3** (C).

(D–F) Theoretical transfer characteristics for molecules **1** (D), **2** (E), and **3** (F). $V_D$ is varied from −0.1, −0.2, −0.4, −0.6 to −0.8 V in (A)–(F).

molecule **1**. Furthermore, two conductance valleys can be obviously observed from $J_D$-$V_G$ curves, especially at $V_D$ = –0.1 V, which is due to the QI-induced conductance minima for molecule **2**. This is clear from the theoretical transfer characteristics ($I_D$-$V_G$) of molecule 2 (Figure 6E), where two conductance valleys appear and become mixed together with $V_D$ changing from –0.1 to –0.8 V. Furthermore, the on-off ratio decreases with increasing $|V_D|$, which can be attributed to electron transmission occurring over a wider bias window, with the conductance being less sensitive to gating-induced movement of molecular energy levels. Similar transfer characteristics appear for molecule 3 (Figure 6C), and the highest on-off ratio is further increased to 306 near $V_D$ = 0 V (Figure S28F), which is about 2.9 times the value for molecule **2** and 12.0 times the value for molecule **1**. This is consistent with the theoretical transfer characteristics ($I_D$-$V_G$) of molecule **3** (Figure 6C) because two conductance valleys appear and the on-off ratios decrease as $V_D$ changes from –0.1 to –0.8 V.

## DISCUSSION

In summary, we have demonstrated that unequivocal signatures of single-molecule room-temperature QI can be translated into self-assembled molecular films. Furthermore, anthanthrene-based molecular transistors, formed from vertical cross-plane graphene/SAM/gold heterostructures and ionic liquid gating, are shown to exhibit stable room-temperature switching operations. Using two different connectivities to the anthanthrene core, QI effects lead to a conductance ratio of approximately 34 for molecular junctions **1** and **2**, which can be further increased to 173 for junction **3** by controlling the molecule-electrode interface with different terminal groups. It should be noted that all three studied molecules exhibit constructive QI. For graphene-like molecules, the term "destructive QI" is conventionally applied to connectivities for which counting rules[34] identify a zero in the transmission

coefficient near the middle of their HOMO-LUMO gap. Equivalently, this would mean that the corresponding magic number vanishes. For the two connectivities considered here, the magic numbers and mid-gap transmissions are non-zero, therefore the molecules with different connectivities exhibit different degrees of constructive QI. Importantly, junction **3** can show a significant current modulation by an ionic liquid gate, with a maximum on-off ratio up to 306, which is about one order of magnitude higher than that for **1**. This enhanced gate behavior for molecule **3** is a direct consequence of the zero-bias conductance suppression induced by QI, combined with a higher interfacial resistance. The designed QI-controlled molecular transistors with large on-off ratio are potential electronic building blocks for future integrated circuits and functional ultra-thin film materials. From the viewpoint of fundamental science, the advantage is that incorporating a molecular layer in a graphene-FET device enables this first demonstration that constructive QI effects are preserved in SAMs. This is significant because it means that QI-based strategies for enhancing monolayer materials properties such as the electrical conductance, thermal conductance, and Seebeck coefficient of SAMs can be pursued in the future with confidence. From a g-FET device viewpoint, QI-SAMs can improve intrinsic field-effect properties and expand other functionalities of the device.

## EXPERIMENTAL PROCEDURES

Full experimental procedures are provided in the Supplemental Information.

## SUPPLEMENTAL INFORMATION

Supplemental Information includes Supplemental Experimental Procedures, 33 figures, 1 scheme, and 1 table and can be found with this article online at https://doi.org/10.1016/j.chempr.2018.12.008.

## ACKNOWLEDGMENTS

We acknowledge the Nanoelectronics Research Facility (NRF) at UCLA for technical support. X.D. acknowledges financial support by ONR through grant number N00014-15-1-2368. Support from the UK EPSRC is acknowledged, through grant numbers EP/N017188/1, EP/P027156/1, and EP/N03337X/1. Support from the European Commission is provided by the FET Open project 767187–QuIET and the EU project BAC-TO-FUEL.

## AUTHOR CONTRIBUTIONS

X.D., C.L., and C.J. conceived and designed the experiments. C.J. performed most of the experiments, including device fabrication, characterization, and data analysis. M.F. and I.M.G. performed the theoretical simulation and data analysis. X.L., S.D., and S.-X.L. synthesized the molecules. P.W., J.G., Y.L., and Z.F. assisted with device fabrication and characterizations. Y.W. performed the AFM studies. Z.Z. performed the XPS studies. X.D., C.L., R.H., S.-X.L., and Y.H. supervised the research. X.D., C.L., C.J., S.-X.L., and M.F. co-wrote the paper. All authors discussed the results and commented on the manuscript.

## DECLARATION OF INTERESTS

The authors declare no competing financial interests.

Received: September 6, 2018
Revised: November 26, 2018
Accepted: December 11, 2018
Published: January 24, 2019

## REFERENCES AND NOTES


1. Aradhya, S.V., and Venkataraman, L. (2013). Single-molecule junctions beyond electronic transport. Nat. Nanotechnol. *8*, 399–410.
2. Lambert, C.J. (2015). Basic concepts of quantum interference and electron transport in single-molecule electronics. Chem. Soc. Rev. *44*, 875–888.
3. Xiang, D., Wang, X., Jia, C., Lee, T., and Guo, X. (2016). Molecular-scale electronics: From concept to function. Chem. Rev. *116*, 4318–4440.
4. Jia, C., Migliore, A., Xin, N., Huang, S., Wang, J., Yang, Q., Wang, S., Chen, H., Wang, D., Feng, B., et al. (2016). Covalently bonded single-molecule junctions with stable and reversible photoswitched conductivity. Science *352*, 1443–1445.
5. Magoga, M., and Joachim, C. (1999). Conductance of molecular wires connected or bonded in parallel. Phys. Rev. B *59*, 16011–16021.
6. Papadopoulos, T.A., Grace, I.M., and Lambert, C.J. (2006). Control of electron transport through Fano resonances in molecular wires. Phys. Rev. B *74*.
7. Markussen, T., Schiötz, J., and Thygesen, K.S. (2010). Electrochemical control of quantum interference in anthraquinone-based molecular switches. J. Chem. Phys. *132*.
8. Vazquez, H., Skouta, R., Schneebeli, S., Kamenetska, M., Breslow, R., Venkataraman, L., and Hybertsen, M.S. (2012). Probing the conductance superposition law in single-molecule circuits with parallel paths. Nat. Nanotechnol. *7*, 663–667.
9. Ballmann, S., Härtle, R., Coto, P.B., Elbing, M., Mayor, M., Bryce, M.R., Thoss, M., and Weber, H.B. (2012). Experimental evidence for quantum interference and vibrationally induced decoherence in single-molecule junctions. Phys. Rev. Lett. *109*.
10. Aradhya, S.V., Meisner, J.S., Krikorian, M., Ahn, S., Parameswaran, R., Steigerwald, M.L., Nuckolls, C., and Venkataraman, L. (2012). Dissecting contact mechanics from quantum interference in single-molecule junctions of stilbene derivatives. Nano Lett. *12*, 1643–1647.
11. Kaliginedi, V., Moreno-García, P., Valkenier, H., Hong, W., García-Suárez, V.M., Buiter, P., Otten, J.L.H., Hummelen, J.C., Lambert, C.J., and Wandlowski, T. (2012). Correlations between molecular structure and single-junction conductance: A case study with oligo(phenylene-ethynylene)-type wires. J. Am. Chem. Soc. *134*, 5262–5275.
12. Arroyo, C.R., Tarkuc, S., Frisenda, R., Seldenthuis, J.S., Woerde, C.H.M., Eelkema, R., Grozema, F.C., and van der Zant, H.S.J. (2013). Signatures of quantum interference effects on charge transport through a single benzene ring. Angew. Chem. *125*, 3234–3237.
13. Guédon, C.M., Valkenier, H., Markussen, T., Thygesen, K.S., Hummelen, J.C., and Van Der Molen, S.J. (2012). Observation of quantum interference in molecular charge transport. Nat. Nanotechnol. *7*, 305–309.
14. Ke, S.-H., Yang, W., and Baranger, H.U. (2008). Quantum-interference-controlled molecular electronics. Nano Lett. *8*, 3257–3261.
15. Zhang, Y., Ye, G., Soni, S., Qiu, X., Krijger, T.L., Jonkman, H.T., Carlotti, M., Sauter, E., Zharnikov, M., and Chiechi, R.C. (2018). Controlling destructive quantum interference in tunneling junctions comprising self-assembled monolayers via bond topology and functional groups. Chem. Sci. *9*, 4414–4423.
16. Geng, Y., Sangtarash, S., Huang, C., Sadeghi, H., Fu, Y., Hong, W., Wandlowski, T., Decurtins, S., Lambert, C.J., and Liu, S.X. (2015). Magic ratios for connectivity-driven electrical conductance of graphene-like molecules. J. Am. Chem. Soc. *137*, 4469–4476.
17. Sangtarash, S., Huang, C., Sadeghi, H., Sorohhov, G., Hauser, J., Wandlowski, T., Hong, W., Decurtins, S., Liu, S.X., and Lambert, C.J. (2015). Searching the hearts of graphene-like molecules for simplicity, sensitivity, and logic. J. Am. Chem. Soc. *137*, 11425–11431.
18. Lambert, C.J., and Liu, S.X. (2018). A magic ratio rule for beginners: a chemist's guide to quantum interference in molecules. Chem. Eur. J. *24*, 4193–4201.
19. Jia, C., and Guo, X. (2013). Molecule–electrode interfaces in molecular electronic devices. Chem. Soc. Rev. *42*, 5642–5660.
20. Hong, W., Manrique, D.Z., Moreno-García, P., Gulcur, M., Mishchenko, A., Lambert, C.J., Bryce, M.R., and Wandlowski, T. (2012). Single molecular conductance of tolanes: Experimental and theoretical study on the junction evolution dependent on the anchoring group. J. Am. Chem. Soc. *134*, 2292–2304.
21. Moth-Poulsen, K., and Bjørnholm, T. (2009). Molecular electronics with single molecules in solid-state devices. Nat. Nanotechnol. *4*, 551–556.
22. Huang, C., Rudnev, A.V., Hong, W., and Wandlowski, T. (2015). Break junction under electrochemical gating: Testbed for single-molecule electronics. Chem. Soc. Rev. *44*, 889–901.
23. Li, Z., Li, H., Chen, S., Froehlich, T., Yi, C., Schönenberger, C., Calame, M., Decurtins, S., Liu, S.X., and Borguet, E. (2014). Regulating a benzodifuran single molecule redox switch via electrochemical gating and optimization of molecule/electrode coupling. J. Am. Chem. Soc. *136*, 8867–8870.
24. Liu, Y., Weiss, N.O., Duan, X., Cheng, H.-C., Huang, Y., and Duan, X. (2016). Van der Waals heterostructures and devices. Nat. Rev. Mater. *1*, 16042.
25. Novoselov, K.S., Mishchenko, A., Carvalho, A., and Castro Neto, A.H. (2016). 2D materials and van der Waals heterostructures. Science *353*, aac9439.
26. Love, J.C., Estroff, L.A., Kriebel, J.K., Nuzzo, R.G., and Whitesides, G.M. (2005). Self-assembled monolayers of thiolates on metals as a form of nanotechnology. Chem. Rev. *105*, 1103–1170.
27. Ueno, K., Nakamura, S., Shimotani, H., Yuan, H.T., Kimura, N., Nojima, T., Aoki, H., Iwasa, Y., and Kawasaki, M. (2011). Discovery of superconductivity in KTaO3 by electrostatic carrier doping. Nat. Nanotechnol. *6*, 408–412.
28. Tian, T., Rice, P., Santos, E.J.G., and Shih, C.J. (2016). Multiscale analysis for field-effect penetration through two-dimensional materials. Nano Lett. *16*, 5044–5052.
29. Jia, C., Jiang, J., Gan, L., and Guo, X. (2012). Direct optical characterization of graphene growth and domains on growth substrates. Sci. Rep. *2*, 707.
30. Obersteiner, V., Egger, D.A., and Zojer, E. (2015). Impact of anchoring groups on ballistic transport: single molecule vs monolayer junctions. J. Phys. Chem. C *119*, 21198–21208.
31. Sato, T., Masuda, G., and Takagi, K. (2004). Electrochemical properties of novel ionic liquids for electric double layer capacitor applications. Electrochim. Acta *49*, 3603–3611.
32. Ferrer, J., Lambert, C.J., García-Suárez, V.M., Manrique, D.Z., Visontai, D., Oroszlany, L., Rodríguez-Ferradás, R., Grace, I., Bailey, S.W.D., Gillemot, K., et al. (2014). Gollum: A next-generation simulation tool for electron, thermal and spin transport. New J. Phys. *16*.
33. Yu, W.J., Li, Z., Zhou, H., Chen, Y., Wang, Y., Huang, Y., and Duan, X. (2013). Vertically stacked multi-heterostructures of layered materials for logic transistors and complementary inverters. Nat. Mater. *12*, 246–252.
34. Markussen, T., Stadler, R., and Thygesen, K.S. (2010). The relation between structure and quantum interference in single molecule junctions. Nano Lett. *10*, 4260–4265.